Kinetic Origin of Divergent Decompression Pathways in Silicon and Germanium

Jian-Tao Wang, Changfeng Chen, Hiroshi Mizuseki, and Yoshiyuki Kawazoe

Kinetic Origin of Divergent Decompression Pathways in Silicon and Germanium

Jian-Tao Wang,[1, 2, *] Changfeng Chen,[2] Hiroshi Mizuseki,[3] and Yoshiyuki Kawazoe[3, 4]

[1]*Beijing National Laboratory for Condensed Matter Physics,
Institute of Physics, Chinese Academy of Sciences, Beijing 100190, China*
[2]*Department of Physics and High Pressure Science and Engineering Center,
University of Nevada, Las Vegas, Nevada 89154, USA*
[3]*Institute for Materials Research, Tohoku University, Sendai, 980-8577, Japan*
[4]*New Industry Creation Hatchery Center, Tohoku University, Sendai, 980-8579, Japan*

Silicon and germanium transform from diamond to β-tin structure under compression, but upon decompression they turn into metastable BC8 Si and ST12 Ge phases, respectively, instead of returning to the lowest-enthalpy diamond structure. Here we explore by first-principles calculations the atomistic mechanism underlying this intriguing phenomenon. We identify a body-centered tetragonal structure in $I4_1/a$ (C_{4h}^6) symmetry as a precursory state of the BC8 Si phase formed via a double cell bond-rotation mechanism with a low kinetic barrier. Kinetics also play a central role in selecting the decompression pathway in Ge via a trinary cell bond-twisting reconstruction process toward the ST12 Ge phase. In both cases, transformation back to energetically more favorable diamond structure is inhibited by the higher enthalpy barrier. These results explain experimental findings and highlight the kinetic origin of the divergent decompression pathways in Si and Ge.

Group IV elemental (C, Si, Ge) solids exhibit a rich variety of pressure induced structural phase transitions. While they share many structural features because of their common covalent bonding nature, they also show distinct characteristics that reflect their subtle differences in the underlying physics that govern the energetic and kinetic aspects of the phase transformation process. At ambient conditions carbon exists in the form of graphite that transforms at room temperature to diamond-like structures at pressures above 15 GPa [1]. These structural transformations are reversible, and upon decompression graphite is recovered [2]. More intriguing, however, are the phase transitions of silicon and germanium that crystallize at ambient conditions in the cubic diamond structure (Si-I or Ge-I) and transform to a body-centered tetragonal β-tin structure (Si-II or Ge-II) at $\sim$ 11.7 GPa and $\sim$ 9.7 GPa, respectively [3–7]. Upon slow decompression, instead of returning to the most stable diamond structure, divergent transformation pathways lead to a body-centered cubic structure (BC8) for silicon [8–11] or a simple tetragonal structure (ST12) for germanium [11–14]. Despite numerous past theoretical studies on phase stability, the atomistic mechanisms for these complicated decompression induced phase transformations and the corresponding lowest-enthalpy structural conversion pathways remain largely unexplored [15–21].

In this Letter, we report on a first-principles study of energetics and kinetics for the phase transition upon decompression in Si and Ge from the β-tin phase. We focus on the bond reconstruction processes that lead to the transitions from the β-tin phase toward the BC8, ST12 and diamond structure. In particular, we track the enthalpy change along various transformation pathways, examining not only the enthalpy difference of the end-structures, which is the commonly used criterion in evaluating phase transitions, but also the kinetic barriers along the pathways that provide crucial insights into relative competitiveness of different phase transition pathways. Using this approach, we have identified a body-centered tetragonal structure in $I4_1/a$ (C_{4h}^6) symmetry that acts as a precursory state of the BC8 Si phase; this new structure has a small conversion barrier and a small lattice distortion from the β-tin phase via a double cell in-plane local-bond-rotation reconstruction mechanism. The kinetics of the pathway toward the BC8 Si is more favorable than that to the most stable diamond structure. We find that a similar phase transition is also viable in Ge under special conditions (e.g., rapid pressure release [14]); however, a trinary cell local-bond-twisting reconstruction pathway toward the ST12 phase is energetically more favorable and kinetically competitive, making it the dominant pathway in Ge. The favorable kinetics is also the origin of the divergent pathway to the ST12 Ge phase over that to the diamond structure. Our results provide a comprehensive understanding of the experimental findings, underscoring the important role of kinetics in determining phase transformation in Si and Ge.

Our calculations are carried out using density functional theory as implemented in the Vienna *ab initio* simulation package (VASP) [22] with the generalized gradient approximation (GGA) developed by Perdew and Wang [23]. The all-electron projector augmented wave (PAW) method [24] was adopted with $3s^2 3p^2$ for Si and $3d^{10} 4s^2 4p^2$ for Ge treated as valence electrons. A plane-wave basis set with an energy cutoff of 500 eV was used. Forces on the ions are calculated through the Hellmann-Feynman theorem allowing a full geometry optimization. Convergence criteria employed for both the electronic and the ionic relaxation were set to 10^{-6} eV and 0.02 eV/Å for energy and force, respectively.
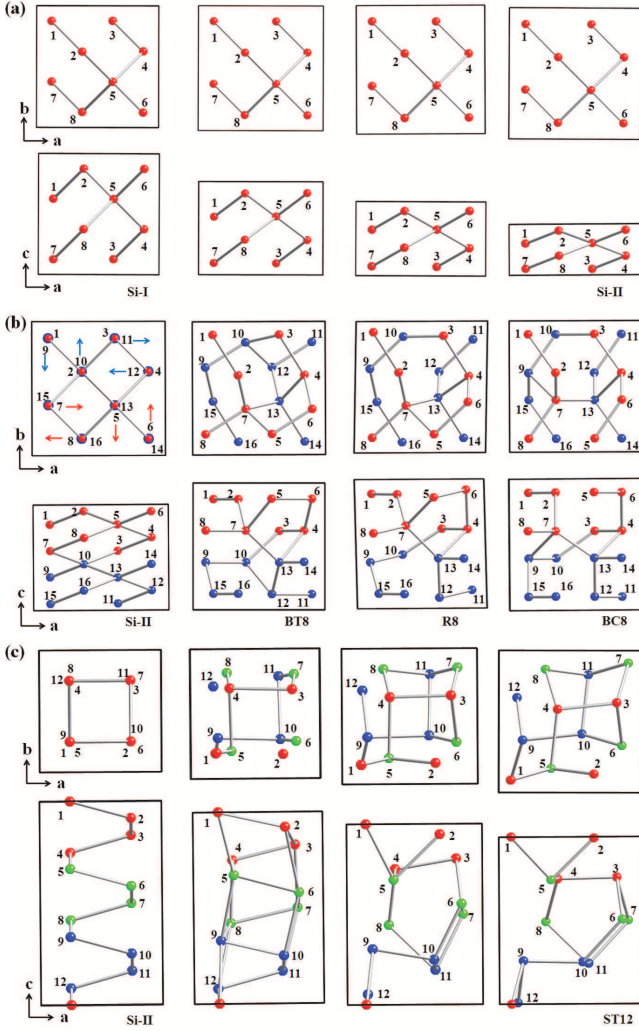
FIG. 1: (color online) (a) Compressed phase conversion process from Si-I to Si-II. Si-I: a cubic diamond structure in $Fd\bar{3}m$ (O_h^7) symmetry; Si-II: a diamond-like superlattice in $I4_1/amd$ (D_{4h}^{19}) symmetry. (b) Local-bond-rotation reconstruction process from Si-II to BC8 via BT8 and R8 phase. Si-II: a 16-atom tetragonal supercell in $I4_1/amd$ (D_{4h}^{19}) symmetry containing two compressed diamond cells along the $c[001]$ direction; BT8: a body-centered tetragonal structure in $I4_1/a$ (C_{4h}^6) symmetry; R8: a distorted body-centered rhombohedral structure in $R\bar{3}$ (C_{3i}^2) symmetry; BC8: a body-centered-cubic structure in $Ia\bar{3}$ (T_h^7) symmetry. (c) Local-bond-twisting reconstruction process from Si-II to ST12. Si-II: a 12-atom tetragonal supercell in $I4_1/amd$ (D_{4h}^{19}) symmetry containing three conventional unit cells of Si-II along the $c[001]$ direction; ST12 in $P4_32_12$ (D_4^8) symmetry.

The cold-compressed (at room temperature) phase transformation from Si-I to Si-II can be described as a lattice distortion process using a single diamond unit cell. Si-II is a compressed diamond-like superlattice with a c/a ratio of 0.39 as shown in Fig. 1(a) with lattice parameters $a_{II} = a_I/\sqrt{2}$ and $c_{II} = c_I$. By changing of the c/a ratio from 1 to 0.39, a conversion barrier is estimated to be 0.25

TABLE I: Calculated equilibrium lattice parameters a, c (in Å), γ (^{o}) and density (ρ in g/cm^3) for Si-I, II, BT8, R8 and BC8 phase at 0, 8 or 12 GPa, compared to available experimental data for Si-I, II, R8 and BC8 phases [3, 10, 11, 28].

Phase	Method	a (Å)	c (Å)	γ (^{o})	ρ (g/cm^3)
I	Cal. (0 GPa)	5.467			2.282
	Exp.[28]	5.431			2.340
II	Cal. (0 GPa)	4.813	2.671		3.015
	Cal. (12 GPa)	4.681	2.573		3.309
	Exp.[3]	4.686	2.585		3.287
BT8	Cal. (0 GPa)	6.684	6.529		2.558
	Cal. (8 GPa)	6.530	6.277		2.787
R8	Cal. (0 GPa)	5.774		109.85	2.554
	Cal. (8 GPa)	5.626		109.99	2.776
	Exp.[10]	5.609		110.07	
BC8	Cal. (0 GPa)	6.663			2.522
	Exp.[11]	6.636			2.553

eV at about 12 GPa. During the entire conversion process the structures remain in $I4_1/amd$ (D_{4h}^{19}) symmetry as in Si-II, and no atomic displacements occur. Based on the same distortion pathway, the conversion barrier from Ge-I to Ge-II is estimated to be 0.22 eV at 9.73 GPa.

We next explore the atomistic mechanism underlying the phase transformation from Si-II toward the BC8 phase in silicon. We examine the kinetic process at the atomic scale using a modified climbing image nudged elastic band method [25–27] with the cell and atomic positions optimization under a wide pressure range of 2∼12 GPa. Because the BC8 phase has a 16 atom cubic unit cell, a 16-atom tetragonal supercell containing four conventional unit cells of Si-II is used to simulate the initial Si-II state. It also can be considered as a double cell of the compressed diamond superlattice along the $c[001]$ direction [see Fig. 1(b)]. Surprisingly, our simulations yield two intermediate metastable phases between Si-II and BC8 [see Fig. 1(b)]. The first one has a body-centered tetragonal structure in $I4_1/a$ (C_{4h}^6) symmetry with lattice parameters a = 6.684 Å and c/a =0.977 and Si atoms occupying the 16f (0.0964, 0.6506, 0.0090) position at 0 GPa. Like BC8, this new structure (termed tetragonal BT8 silicon hereafter) also has eight atoms per primitive cell (a = 5.744 Å, α = 108.845, γ = 110.73^o). The second intermediate phase has a distorted body-centered rhombohedral structure in $R\bar{3}$ (C_{3i}^2) symmetry with lattice parameters a = 6.637 Å, γ = 90.81^o at 0 GPa. This structure is the so-called R8 or Si-XII phase [10], which contains eight atoms per primitive cell (a = 5.774 Å, γ = 109.85^o). Along the phase transformation pathway, a strong *in-plane local-bond-rotation reconstruction* mechanism emerges with the largest displacement of 0.25 unit cell along the in-plane a or b-axis and a small displacement of 0.0625 unit cell parallel to the c-axis.

The calculated lattice parameters for Si-I, II, BT8, R8 and BC8 structures at 0, 8 or 12 GPa are summarized in Table I. They are all in good agreement with the available experimental data [3, 10, 11, 28]. The R8, BC8, and BT8 phases of silicon have almost the same density that is $\sim 22\%$ larger than that of the diamond structure. In contrast to the large lattice distortion during the compression process from Si-I (a =5.467 Å and c/a = 2.0) to Si-II (a = 6.662 Å and c/a = 0.78 at 12 GPa within a double cell of diamond-like structure), upon decompression from Si-II to BC8 (a = 6.663 Å and c/a = 1.0 at 0 GPa), there is a $\sim 22\%$ c-axis expansion, but the change of the in-plane lattice parameter a is very small. This result suggests that the large in-plane lattice expansion of the Si-II phase has created ample space for the local bond rotation during the structural transition. Moreover, the highly symmetric bond rotation can always introduce a certain path toward the decompressed BT8, R8 and BC8 phases (see supplementary material Fig. S1 and Fig. S2).

Figure 2(a) shows the relative enthalpy change along the local bond rotation pathway from Si-II toward the BC8 phase at 8 GPa. The enthalpy increases initially due to the bond twisting and breaking in Si-II phase and then it decreases with the formation of the intermediate BT8 phase. The conversion barrier is estimated to be $\sim$ 0.16 eV, and this low kinetic barrier suggests that the *local bond rotation* can easily take place in the double cell compressed diamond superlattice. Meanwhile, the BT8 structure has the same enthalpy as the R8 phase and can convert to the R8 phase with a very small barrier of $\sim$ 0.03 eV. Experimentally, the R8 phase has been observed in the pressure range 9.3 to 2.8 GPa [9, 10], which is in excellent agreement with our calculated enthalpy results [see Fig. 2(b)]. Our calculations also show that as pressure drops below 2.5 GPa, the R8 phase becomes less stable than the BC8 phase and a conversion to the BC8 phase is expected at ambient conditions, which is again in agreement with the experimental findings [9]. Our results indicate that the first-stage conversion Si-II $\rightarrow$ BT8 is a robust structural reconstruction process along the multistage reaction pathway, and the BT8 phase plays a key role in linking the Si-II and BC8 phases.

We also explored possible transformation pathways for Si-II $\rightarrow$ ST12 with a *local-bond-twisting* reconstruction mechanism within a 12-atoms tetragonal supercell. The detailed reconstruction patterns are shown in Fig. 1(c). The initial Si-II structure contains three conventional unit cells of Si-II along the c-axis. Throughout the transformation pathway, the largest in-plane atomic displacement is about 0.16 unit cell around the (0.25,0.25,z), (0.75,0.25,z), (0.25,0.75,z), and (0.75,0.75,z) positions, and the largest c-axis displacement is about 0.06 unit cell. During the entire process, the structures remain in $P4_32_12$ (D_4^8) symmetry, which is the same as that of the ST12 phase, resulting in a smooth conversion process. However, in contrast to the multistage pathway Si-II $\rightarrow$
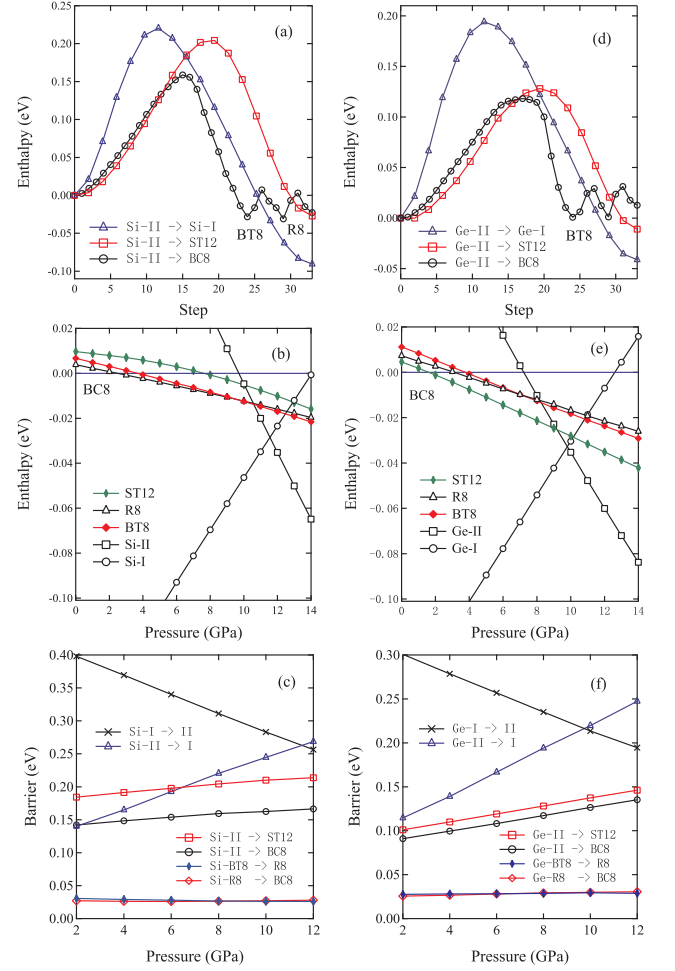

FIG. 2: (color online) (a) Enthalpy versus transformation pathway Si-II $\rightarrow$ BT8 $\rightarrow$ R8 $\rightarrow$ BC8 and Si-II $\rightarrow$ ST12 in competition with Si-II $\rightarrow$ Si-I at 8 GPa. (b) Variation of the enthalpy with pressure for each of the Si phases under consideration, measured with respect to that of the BC8-Si phase. (c) Enthalpy barriers versus pressure for Si-II $\rightarrow$ Si-I, ST12, BC8; BT8 $\rightarrow$ R8; and R8 $\rightarrow$ BC8. (d) Enthalpy versus transformation pathway Ge-II $\rightarrow$ BT8 $\rightarrow$ R8 $\rightarrow$ BC8 and Ge-II $\rightarrow$ ST12 in competition with Ge-II $\rightarrow$ Ge-I at 8 GPa. (e) Variation of the enthalpy with pressure for each of the Ge phases under consideration, measured with respect to that of the BC8-Ge phase. (f) Enthalpy barriers versus pressure for Ge-II $\rightarrow$ Ge-I, ST12, BC8; BT8 $\rightarrow$ R8; and R8 $\rightarrow$ BC8.

BT8 $\rightarrow$ R8 $\rightarrow$ BC8, the pathway toward the ST12 phase is clearly unfavorable with a larger conversion barrier of $\sim$ 0.21 eV [see Fig. 2(a,c)] and higher enthalpy [see Fig. 2(b)]. For comparison, we also plot the enthalpy along the counterreaction pathway Si-II $\rightarrow$ Si-I; it is clearly unfavorable due to the high reaction barrier [see Fig. 2(a,c)] and larger lattice distortion [see Fig. 1(a)]. Thus, the structural reconstruction toward the BC8 phase via a double cell *in-plane local-bond-rotation* mechanism is the lowest-enthalpy phase transition path in silicon, and it prevents the returning to the most stable diamond struc-

ture upon decompression. These results highlight the crucial role of kinetics in selecting favorable pathways.

We now turn to the structural phase transition of Ge upon decompression. We plot the enthalpy along the pathway from Ge-II to Ge-I, ST12, and BC8 at 8 GPa in Fig. 2(d). We find a similar multistage pathway Ge-II → BT8 → R8 → BC8. However, unlike the situation for Si, there is a strong competition from another transformation pathway Ge-II → ST12 with a conversion barrier of 0.128 eV, which is only slightly higher that the barrier of 0.117 eV for the pathway Ge-II → BC8. Meanwhile, the critical transition pressures are estimated to be 9.2 GPa for Ge-II → ST12 and 8.3 GPa for Ge-II → BT8. Therefore, the structural transition to BC8 Ge via the intermediate BT8 Ge structure has a small kinetic advantage but is not energetically favorable and, consequently, the BC8 Ge phase can only be realized under special conditions such as a rapid pressure release when the system has a chance to cross the low kinetic barrier as observed in experiment [14]. Under slow pressure release from the high-pressure β-tin phase, only ST12 germanium is expected to be present in a wide pressure range of 9.2 ~ 1.6 GPa since the ST12 phase is kinetically competitive and energetically more favorable than the BC8 phase [see Fig. 2(e,f)], which again is in agreement with the experimental observation [14]. Similar to the results for Si-II → Si-I, our calculations show that the counterreaction from Ge-II to revert to Ge-I is inhibited by a higher kinetic barrier[see Fig. 2(d,f)]. The distinction between the local bond rotation in Si toward BC8 and local bond twist-

ing in Ge toward ST12 phase stems from the difference in the relative bond strength, where the stronger Si-Si bonds are harder and thus tend to rotate more rigidly while the weaker Ge-Ge bonds are more susceptible to deformation in the form of bond twisting.

It should be noted that pressure has little effect on the relative enthalpy and conversion barrier during the decompression conversion process toward the BC8 and ST12 phase [see Fig. 2(b,c,e,f)]. Similar behavior is also found between the diamond-like dense phase conversions [26]. The pathways toward the BC8 or ST12 phases are more favorable than phase-II → phase-I in a wide pressure range of 2 ~ 12 GPa in Si and Ge [see Fig. 2(c,f)]. Meanwhile, the kinetic barriers for the structural transformations between BT8-R8 and R8-SC8 phases are actually small (~ 0.03 eV), which suggests that these intermediate phases are highly susceptible to changes in the structural and pressure conditions.

Figure 3 shows the simulated x-ray diffraction (XRD) patterns for the Si-I, Si-II, BT8, R8 and BC8 phases, compared to the experimental data for silicon on pressure decrease from 12.7 GPa [9]. On increasing pressure, the main peak (111) at 8.2^o in Si-I splits into two peaks, (200) and (101), around 11.4^o and 11.8^o in Si-II phase at 12 GPa. Upon decompression from Si-II, a broad peak (211) appear at 10° in the BT8 phase. From the BT8 toward the BC8 phase, the main peak (211) becomes sharper due to the increasing atomic order and lattice symmetry. The BT8, R8, and BC8 phases have similar XRD patterns due to the close atomic density and structure. Meanwhile, the small changes in the Si-Si bond lengths, bond angles and lattice symmetry induce two small peaks at 5.7^o and 8°, which are consistent with the experimental findings [9] [see Fig. 3(b)]. These results suggest that the BT8 structure is among the likely candidate phases of Si upon decompression from the β-tin phase [29]. Furthermore, the calculated phonon dispersion curves and electronic band structure show that the BT8 phase is dynamically stable and exhibits semimetallic character (see supplementary material Fig. S3) that is similar to those of the R8 and BC8 phase [30].

In summary, we have performed first-principles calculations to probe the atomistic reconstruction mechanisms for the irreversible structural phase transitions of Si and Ge upon decompression from the high-pressure β-tin phase. We have identified two basic reconstruction pathways, one toward the BC8 Si via a double cell *in-plane local-bond-rotation* reconstruction mechanism, and the other toward the ST12 Ge via a trinary cell *local-bond-twisting* reconstruction mechanism. The pathways to return to the most stable diamond structure of Si and Ge are inhibited by the higher kinetic barriers in both cases. Moreover, a metastable tetragonal BT8 structure in $I4_1/a$ symmetry has been identified as an intermediate structure between the Si-II and BC8 Si phase that facilitates the structural reconstruction. This new phase
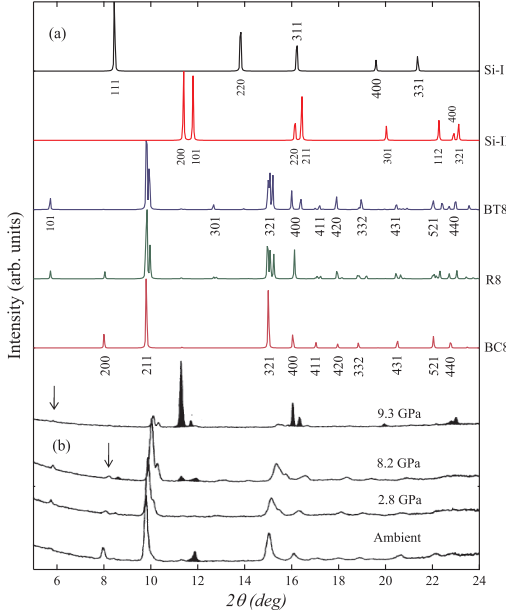

FIG. 3: (color online) (a) Simulated XRD patterns for Si-I, Si-II, BT8, R8 and BC8 phases. (b) Experimental XRD patterns from silicon on pressure decrease from 12.7 GPa [9]. X-ray wavelength is 0.4652 Å.

as a precursory state of the BC8 phase is also viable in Ge under special conditions such as a rapid pressure release; but the primary decompressed ST12 Ge phase dominates when the pressure release is slow and the system has sufficient time to follow the energetically most favorable pathway that is also kinetically competitive. The crucial role of kinetics in selecting the divergent decompression pathways explains the intriguing structural transformations observed in silicon and germanium.

---

[*] e-mail address:wjt@aphy.iphy.ac.cn

[1] M. Amsler, J. A. Flores-Livas, L. Lehtovaara, F. Balima, S. A. Ghasemi, D. Machon, S. Pailhes, A. Willand, D. Caliste, S. Botti, A. SanMiguel, S. Goedecker, and M. A. L. Marques, Phys. Rev. Lett. **108,** 065501 (2012).

[2] W. L. Mao, H. Mao, P. J. Eng, T. P. Trainor, M. Newville, C. Kao, D. L. Heinz, J. Shu, Y. Meng, and R. J. Hemley, Science **302**, 425 (2003).

[3] J. C. Jamieson, Science **139,** 762 (1963).

[4] J. Z. Hu and I. L. Spain, Solid State Commun. **51,** 263 (1984).

[5] M. I. McMahon and R. J. Nelmes, Phys. Rev. B **47,** 8337 (1993).

[6] M. I. McMahon, R. J. Nelmes, N. G. Wright, and D. R. Allan, Phys. Rev. B **50,** 739 (1994).

[7] H. Olijnyk, S. K. Sikka, and W. B. Holzapfel, Phys. Lett. **103A,** 137 (1984).

[8] R. H. Wentorf and J. S. Kasper, Science **139,** 338 (1963).

[9] R. O. Piltz, J. R. Maclean, S. J. Clark, G. J. Ackland, P. D. Hatton, and J. Crain, Phys. Rev. B. **52,** 4072 (1995).

[10] J. Crain, G. J. Ackland, J. R. Maclean, R. O. Piltz, P. D. Hatton, and G. S. Pawley, Phys. Rev. B **50,** 13043 (1994).

[11] J. S. Kasper and S. M. Richards, Acta Cryst. **17,** 752 (1964).

[12] F. P. Bundy and J. S. Kasper, Science **139,** 340 (1963).

[13] H. B. Cui, D. Graf, J. S. Brooks, and H. Kobayashi, Phys. Rev. Lett. **102,** 237001 (2009).

[14] R. J. Nelmes, M. I. McMahon, N. G. Wright, D. R. Allan, and J. S. Loveday, Phys. Rev. B **48,** 9883 (1993).

[15] M. T. Yin, Phys. Rev. B **30,** 1773 (1984).

[16] R. Biswas, R. M. Martin, R. J. Needs, and O. H. Nielsen, Phys. Rev. B **30,** 3210 (1984).

[17] F. Zandiehnadem and W. Y. Ching, Phys. Rev. B **41,** 12162 (1990).

[18] A. Mujica and R. J. Needs, Phys. Rev. B **48,** 17010 (1993).

[19] K. Mizushima, S. Yip, and E. Kaxiras, Phys. Rev. B **50,** 14952 (1994).

[20] K. Gaal-Nagy and D. Strauch, Phys. Rev. B **73,** 134101 (2006).

[21] S. L. Qiu and P. M. Marcus, J. Phys.: Condens. Matter **24,** 225501 (2012).

[22] G. Kresse and J. Furthmüller, Phys. Rev. B **54**, 11169 (1996); G. Kresse and J. Hafner, *ibid.* **47**, 558 (1993).

[23] J. P. Perdew and Y. Wang, Phys. Rev. B **45,** 13244 (1992).

[24] P. E. Blöchl, Phys. Rev. B **50**, 17953 (1994); G. Kresse and D. Joubert, Phys. Rev. B **59**, 1758 (1999).

[25] J. T. Wang, C. F. Chen, and Y. Kawazoe, Phys. Rev. Lett. **106,** 075501 (2011).

[26] J. T. Wang, C. F. Chen, and Y. Kawazoe, Phys. Rev. B **84,** 012102 (2011).

[27] See http://theory.cm.utexas.edu/henkelman for study of the kinetic processes at the atomic scale.

[28] M. E. Straumanis, P. Borgeaud, and W. J. James, J. Appl. Phys. **32,** 1382 (1961).

[29] B. C. Johnson, B. Haberl, J. E. Bradby, J. C. McCallum, and J. S. Williams, Phys. Rev. B **83,** 235205 (2011).

[30] B. D. Malone, J. D. Sau, and M. L. Cohen, Phys. Rev. B **78,** 035210 (2008).